Article

Morphological and Physicochemical Properties of Macrocrystalline Talc from Argentine

Silvia E. Barbosa [1,2,*] **and Luciana A. Castillo** [1,2]

1 Planta Piloto de Ingeniería Química, PLAPIQUI (UNS-CONICET), Cno. La Carrindanga km. 7, Bahía Blanca 8000, Argentina; lcastillo@plapiqui.edu.ar

2 Departamento de Ingeniería Química, Universidad Nacional del Sur (UNS), Av. Alem 1253, Bahía Blanca 8000, Argentina

* Correspondence: sbarbosa@plapiqui.edu.ar

Abstract: A detailed petrographical, mineralogical, morphological, geochemical and physicochemical characterization of talc from an Argentinean ore is presented. This deposit is located in the San Juan province at the foothills of the Andes. Characterization was performed on rock and milled talc using different techniques including polarized light microscopy, transmission electron and scanning microscopy with energy dispersive spectroscopy (SEM/EDX), chemical analyses, X-ray diffraction (XRD), X-ray fluorescence, Fourier transform infrared spectroscopy (FTIR), particle size determination by laser diffraction, thermogravimetry analysis, and colorimetry. A mineral sample contains approximately 80 wt% talc. Associated minerals such as carbonates as veins and chlorite interlaminated with talc were detected. Carbonates are calcite, dolomite and magnesite, as was corroborated by FTIR. Morphology and crystallinity were assessed by XRD data, obtaining a morphological index of 0.79 which indicates the macrocrystalline character. Crystalline habits of associated minerals were recognized by SEM, detecting their constitutive elements by EDX. Talc color parameters are $L^* = 82.76$, $a^* = -1.50$, and $b^* = 5.38$. The slight yellowing could be attributed to chlorite or traces of Fe oxides. Although the whiteness index (62.12) impedes its commercialization as a high-priced mineral, this kind of talc can be used as an additive for polymers, since it would offer a high reinforcing effect (improvement of mechanical properties).

Keywords: talc; macrocrystalline morphology; Argentinean ore; carbonates; mineral characterization; associated minerals

1. Introduction

Geologically, talc occurs in rocks that coexist with other associated minerals such as chlorite, dolomite, magnesite, amphibole, biotite, olivine, pyroxene, quartz, and serpentine [1,2]. Talc deposits differ according to the parent rock from which they are derived. Each ore has its own geological signature formed many millions of years ago. Its formation is related to the transformation of existing mineral species under the effect of hydrothermal fluids that carry one or more of the necessary components (MgO, SiO_2 and H_2O) to form talc. Plate tectonics play a very important role in the genesis of talc deposit, since they allow hydrothermal fluids to penetrate the rock and facilitate reactions in it. The size and shape of a talc deposit depend on the intensity of hydrothermal activity, while the pressures and deformations that occur during and after transformation determine its characteristics.

Talc is a layered silicate (phyllosilicate) and its ideal unit structure is $Mg_3Si_4O_{10}(OH)_2$. The theoretical chemical composition of this mineral contains 63.37% SiO_2, 31.80% MgO, and 4.75% H_2O. It presents a stacked structure where sheets are arranged with a variable degree of disorder, so they can slide easily, giving talc its characteristic softness. Talc sheets have two types of surfaces: "face" and "edge". The first ones contain the basal planes as a consequence of sheets sliding and they have siloxane groups (–Si–O–Si–). Face surfaces are electrically neutral, energetically weak, nonpolar in water, and hydrophobic [3–6]. The

edge surfaces are formed by breaking from the milling and they contain silanol (SiOH) and magnesiol (MgOH) groups, making them polar and hydrophilic. These surfaces are more energetic than the faces, therefore, they are susceptible to undergo hydrolysis and form relatively strong hydrogen bonds with water molecules and polar substances [7–9]. Talc sheets have an elementary structure that consists of an octahedral layer chemically bonded to two tetrahedral layers by oxygen atoms. The interlaminar distance is 9.4 Å, including the two tetrahedral layers attached to the octahedral one and the separation of adjacent sheets by van der Waals forces [10].

Four categories of talc ore can be distinguished depending on the parent rock from which mineral is formed [11]: (a) derived from magnesium carbonates which is generally pure and white, (b) derived from serpentines that is always grey but can be upgraded, (c) derived from alumino–silicate rocks which generally contains chlorite, and (d) derived from magnesium sedimentary deposits. These categories include a wide variety of deposits that differ in mineralogical composition (type and proportion of associated minerals), color (measured in terms of brightness or whiteness), and crystalline morphology. Considering morphological aspects, talc can be classified as either microcrystalline (particle length:thickness = 10:1) or macrocrystalline (particle length:thickness = 35:1) [12]. Mineralogical composition, color and crystalline morphology govern the specific nature of each grade of commercial talc, as well as its industrial applications. Particularly, Argentine has talc deposits in the Mendoza and San Juan provinces, in the foothills of the Andes, and their formation has been assigned to the Upper Paleozoic–Lower Triassic [13–15]. Due to their genesis, talc presents specific characteristics and properties. The aim of this work is to study these properties by different and complementary techniques such as petrographical, mineralogical, morphological, geochemical, and physicochemical analysis in order to determine its potential uses.

2. Materials and Methods

Different representative rock samples were extracted from a talc deposit located in the province of San Juan, which has been circumscribed to the Sierra de Pie de Palo. This orographic subsystem belongs to the Sierras Pampeanas of central–western Argentine. A geological map of this system is reported in Rapela et al. [16]. Talc deposit is 20 km long and 7 km wide. There are bodies of serpentines which are arranged accordingly with veins in lenticular layers hosted in serpentinite bodies or in contact with the bedrock, micacites, and quartzites. Although these bodies have very variable thicknesses, talc veins have an average width of 1 m [17]. All extracted rock samples were crushed, ground for 5 min by means of a micronizing miller, then sieved, and the powder fraction selected (<20 μm). This allows the obtaining of a homogeneous and representative material to perform the analysis.

Talc samples were characterized by complementary and independent techniques to perform a petrographical, mineralogical, morphological, geochemical, and physicochemical analysis.

The petrographic study by polarized light microscopy (PLM) was carried out on three thin sections of six representative samples extracted from the talc rock. To perform this analysis an Olympus SZ-Pt trinocular stereomicroscope and an Olympus B2-UMA trinocular petrographic microscope (Olympus, Tokyo, Japan) were used. Both of them are equipped with a built-in video camera, a digital capture system, and software for image processing.

Bulk mineralogy was determined on talc powder by X-ray diffraction (XRD) using a Rigaku D Max III-C X-ray diffractometer (Rigaku, Tokyo, Japan) set at 35 kV and 15 mA, with CuKα radiation (wavelength of 1.54060 Å) and a graphite monochromator in the secondary diffracted beam to remove CuKβ radiation. Diffractograms were produced ranging 2θ from 3° to 60°, with 0.04° in 2θ increments and a counting time of 1 s per increment, using a slit width of 0.6°. The sample was mounted in a dimpled glass, and then a glass slide was used to press the material and remove the exceeding material.

Identification of minerals was performed by means of JADE software (version 7, ICDD, Newton Square, PA, USA) using the values in counts per second.

Morphological and microchemical analyses were carried out by scanning electron microscopy (SEM) using a JEOL JSM 35 CF microscope (JEOL Ltd., Tokyo, Japan) with an energy dispersive X-ray spectrometer (EDAX 2000, Mahwah, NJ, USA). Before the SEM analysis, samples were coated with a thin gold layer (~30 Å thick) using an argon plasma metallizer (sputter coater PELCO 91000, Fresno, CA, USA) in order to make the sample conductive. This analysis was performed on talc rock and powder.

Talc particle size was measured using a Sedigraph® 5100 from Micromeritics, Norcross, GA, USA. All samples were dispersed with a 0.1% solution of sodium diphosphate. Samples of 10 g dry talc were dispersed in 100 cm^3 of the diphosphate solution with a high-speed blender for 15 min at 15,000 min^{-1} followed by ultrasonication for 10 min in a 130 W ultrasonic bath.

The sheet stacking sequence and order in talc particles were analyzed by transmission electron microscopy (TEM) using a JEOL 100 CX microscope operating at 100 kV. To prepare samples, talc particles were previously embedded in an epoxy resin. Then, thin sections (approximately 600 Å) from the embedded samples were studied by using a Leica ultramicrotome in a perpendicular direction to the particle basal plane. Microscopical observations were performed on these thin sections.

The chemical composition of talc samples was determined with an X-ray fluorescence (XRF) spectrometer (PANalytical Magi'X, Malvern, UK) with a rhodium anode, FLi 200, LiF220, Ge, PX1, PX4, PE analyzer crystals, and flow and scintillation detectors. This analysis was performed under vacuum conditions. The semiquantitative analysis was performed using IQ$^+$ software (version 3.05(3.346.3), PANalytical B.V., Almelo, The Netherlands) integrated with the spectrometer which contains a wide database of patterns and correction coefficients library. The detection limit of this technique is 1 ppm.

Fourier transform-infrared (FTIR) spectra of powdered samples were recorded using a Nicolet 520 FT-IR spectrophotometer (model 520, Thermo Fisher Scientific, Madison, WI, USA) with a DTGS detector. Samples were mixed with spectroscopic grade potassium bromide (KBr) in a ratio of 1:99 (talc:KBr) in an agate mortar. Then, the mixture was placed in a hydraulic press and compressed to produce pellets for recording the spectra. The infrared spectrum range was 400–4000 cm^{-1}, using 32 scans and a resolution of 4 cm^{-1} under nitrogen atmosphere.

Thermogravimetric analysis (TGA) was carried out with a TA Instrument equipment (model Discovery Series). Samples of finely ground talc (<20 μm) powder were heated in the temperature range of 30–1000 °C with a heating rate of 10 °C min^{-1} in a nitrogen atmosphere.

Color properties of talc samples were determined using a Hunterlab UltraScan XE (Reston, VA, USA) colorimeter on a thin disk of compressed powder. *L**, *a**, and *b** values were measured under the standard illuminant D65 by using the CIELAB (Commission Internationale de l´Eclairage *L*a*b**) system. The colorimeter was calibrated to the perfect white diffuser by a ceramic plate. The whiteness index (*WI*) values were calculated by taking the values of the CIELab scale (*L**, *a**, *b**) and the Hunter equation [18], modified by Stensby [19]:

$$WI = L^* - 3b^* + 3a^* \tag{1}$$

3. Results and Discussion

A detailed petrographic analysis of talc rock was performed to identify and describe microscopic characteristics. Figure 1 includes photographs that show optical properties of talc thin sections observed under plane-polarized light and crossed polars. A coarse granulometry and the presence of carbonates can be observed in Figure 1a. Moreover, a dark spot associated with iron oxide presence can be distinguished. Isolated grains with a smooth appearance can be seen distributed within the thin section and they can be related to relics of quartz. The shape of these relics proceeds from the erosion by the forming fluids.

With the aid of cross polars, carbonates are seen in the form of veins and a magnesium-rich chlorite is detected in bluish–gray areas (Figure 1b). Particularly, using polarized light, carbonates are clearly distinguished since they present cleavage lines (Figure 1c). Chlorites and talc are minerals frequently associated as interlaminates in domains one or various layers thick since they occur as a result of hydrothermal alteration [20,21]. Moreover, dark spots are distinguished, and the larger ones are probably holes in the rock cut (Figure 1b). From the petrographical analysis, it can be inferred that the original rock was a carbonite schist, more specifically a calcitic one, so the original carbonate was calcite. Considering this limestone rock and an excess of Mg in the surrounding environment, a substitution by ionic exchange of calcium for magnesium could have led to dolomite formation. This transformation was probably accompanied with a decrease in volume, making crystals grow without a particular direction, as can be seen in the micrographs. Magnesium still in excess could be responsible of magnesite formation in the presence of calcite. Regarding talc formation, it would be associated with an even greater excess of available Mg after the previous transformation.
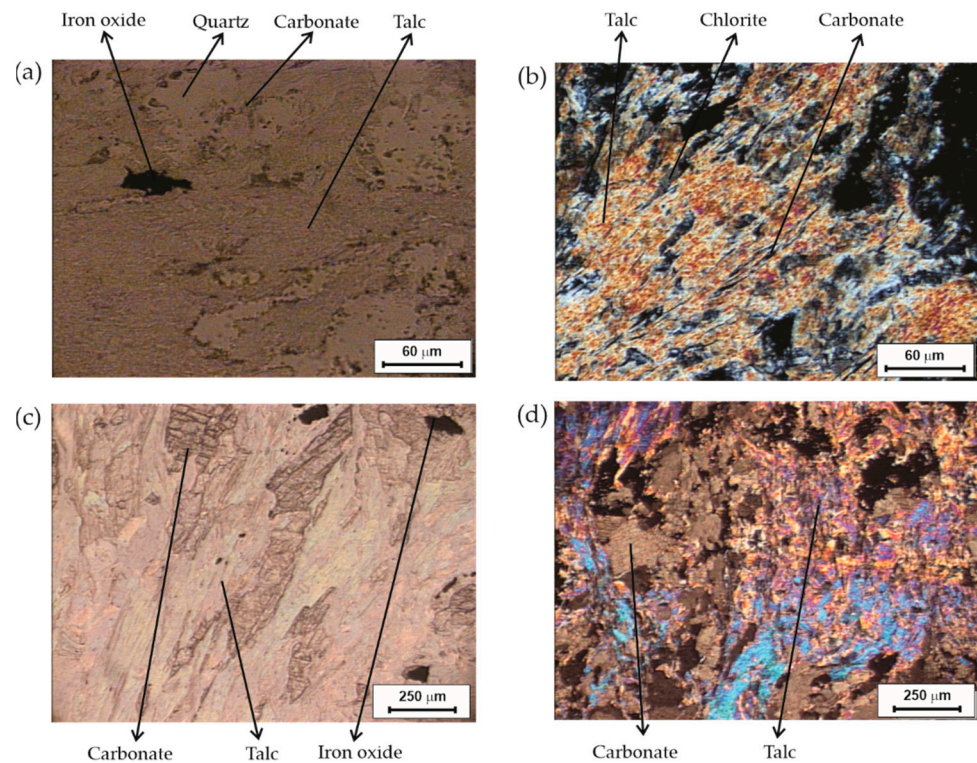

Figure 1. Photographs of thin sections of talc rock observed by an optical microscopy using: (**a**,**c**) plane-polarized light, and (**b**,**d**) crossed polars.

XRD analysis confirms that samples contain talc with associated minerals, as it was previously detected by optical microscopy. Figure 2 presents the diffractogram of powdered talc which includes the peak assignment to the corresponding minerals. The characteristic peaks of talc are associated to d values of 9.44, 4.69 and 3.12 Å, which were assigned to the basal planes (002), (004) and (006), respectively (JCPDS 19-770). The associated minerals detected were chlorite (14.33, 7.16 and 3.56 Å, JCPDS 16-362) and carbonates such as calcite (3.03 Å, JCPDS 5-586), dolomite (2.89 and 1.80 Å, JCPDS 36-426), and magnesite (2.75 and 1.7 Å, JCPDS 8-479). It is important to mention that magnesite is found in a higher proportion than the other carbonates. Moreover, considering the maximum intensity detected (included in Figure 2), talc samples have a high crystallinity.
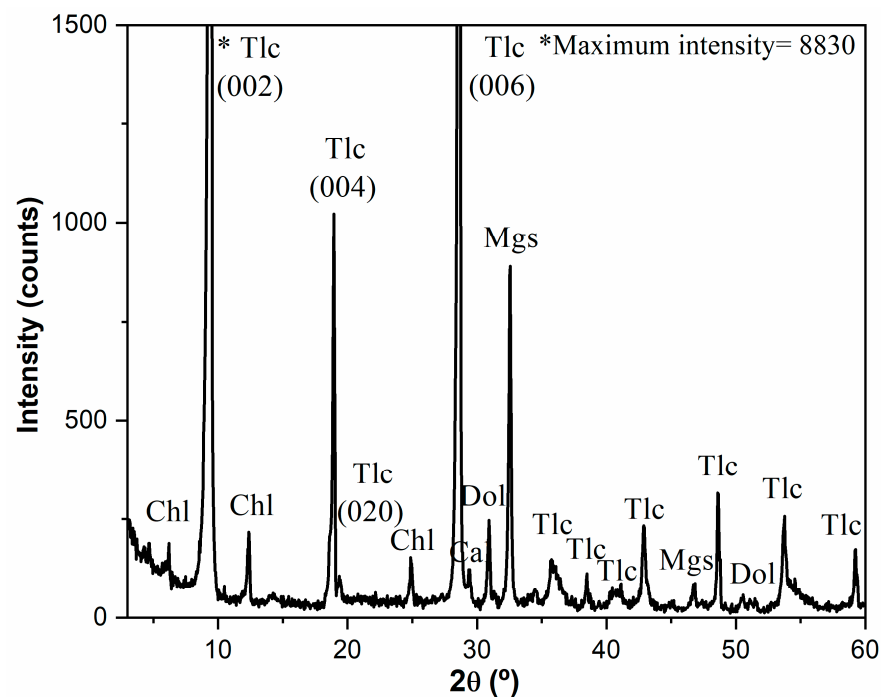
Figure 2. Diffractogram of finely ground talc (<20 μm). Reference: Cal: calcite, Chl: chlorite, Dol: dolomite, Mgs: magnesite and Tlc: talc. (Warr [22]). Reprinted, with permission, from Castillo et al. 2014 © Taylor & Francis.

To analyze talc crystalline morphology, a morphological index (*M*) proposed by Holland and Murtagh [23] was calculated from XRD data. To determine if a talc sample is macro or microcrystalline, they proposed an expression in terms of the intensity of (004) and (020) corresponding to *d* values of 4.69 and 4.61 Å, respectively, as follows:

$$M = \frac{I_x}{I_x + 2I_y} \tag{2}$$

where I_x is the intensity of the (004) reflection and I_y is the intensity of (020).

According to this morphological index, values close to 1 indicate a macrocrystalline character, meanwhile if they are close to 0 it corresponds to a microcrystalline morphology. For this talc sample, the value of *M* is 0.79, revealing a high macrocrystalline character.

Another microstructural feature of talc particles is the crystallite size which is a measure of the size of coherent diffraction domains. This value does not match with particle size due to polycrystalline aggregates. Crystallite size can be determined from XRD data by using the Scherrer equation [24] which is obtained from Bragg's law:

$$D_{(hkl)} = \frac{K\lambda}{FWHM cos(\theta)} \tag{3}$$

where $D_{(hkl)}$ is the average crystallite size measured perpendicular to the family of planes (hkl), *K* is Scherrer's constant with a value of 0.9, *λ* is the wavelength of the incident radiation x, *FWHM* is the width of the peak evaluated at half intensity and *θ* is the angle of maximum intensity of the peak in radians. Since the (002) reflection is one of the most intense for talc [25], the analysis of crystalline size was performed considering this signal. The obtained value for the studied talc sample is 123 nm, which is three times higher than the reported value for ground talc [26]. The diffractogram of Argentinean talc not only reveals a high crystallinity, but also the presence of large crystals.

Morphological study of talc allows the obtaining of information about shape, size and particle size distribution. SEM micrographs of the rock surface and finely ground powder

(<20 μm) were obtained from the same talc ore. A planar habit is observed in Figure 3a, which mainly corresponds to talc and it appears as plates, and flakes with differently sized and layered crystals.
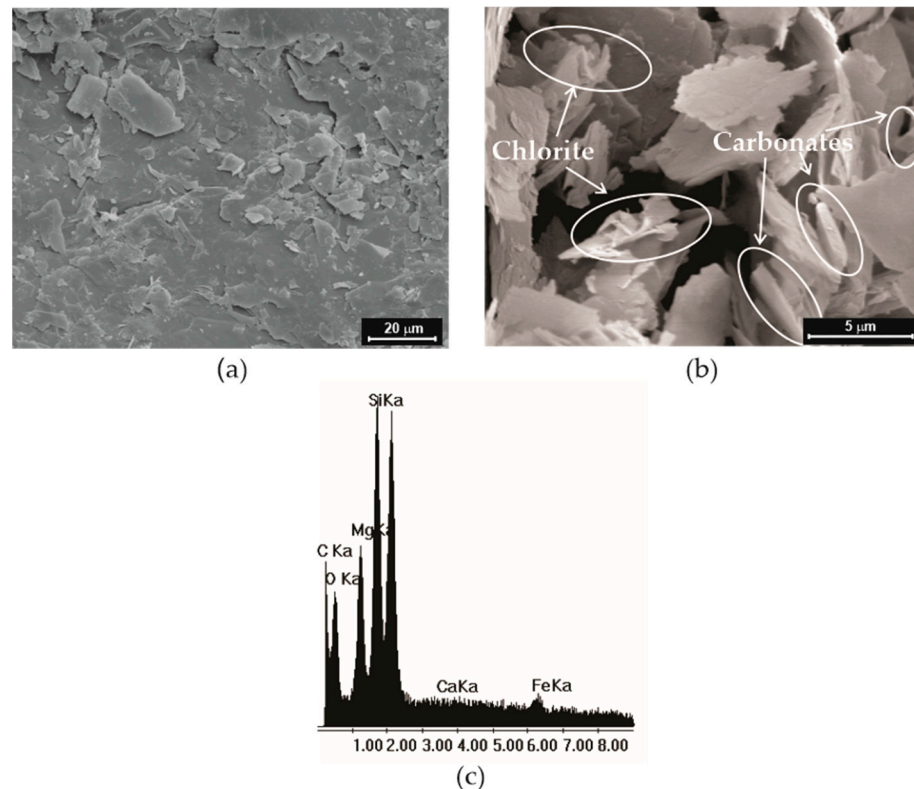

(a)   (b)

(c)

Figure 3. SEM micrographs of: (**a**) talc rock surface, (**b**) finely ground powder (<20 μm), and (**c**) EDX spectrum onto powdered talc.

Milled talc presents particles with prismatic shapes and clear surfaces with defined and abrupt edges (Figure 3b). These features are characteristics of macrocrystalline talc [27]. This morphology is consistent with talc genesis, analogous to that of those minerals from Vermont (Canada), which are macrocrystalline [28]. Associated minerals are randomly distributed in powdered talc as a consequence of the grinding and the mixing during the processing. Carbonates are distinguished by present trigonal geometry and rhombohedral cleavage. Dolomite and calcite are recognized by rhombohedral shapes, while magnesite exhibits anhedral shapes with rhombohedral edges. Chlorite mainly occurs in the form of curved flakes with angular borders. The presence of these associated minerals is also confirmed by the EDX spectra included in Figure 3c. Besides the talc constituent elements such Si, Mg, and O, Ca, Fe, and C are detected, coming from carbonates and chlorite.

Concerning particle size, talc presents a wide monomodal distribution. The obtained values of D10, D50 and D90 by sedigraphy are 2.10 ± 0.54 μm; 5.93 ± 2.52 μm and 11.24 ± 1.56, respectively. D50 values was also assessed by using SEM. This determination was performed considering more than 100 particles on micrographs and registering the maximum length of face surfaces. Data processing was carried out with an Analysis PRO™ software (version 3.0, Soft Imaging System GmbH, Münster, Germany) package. The result of this complementary measurement was 5.86 ± 3.59 μm, in agreement with the sedigraphy value.

Figure 4 shows the TEM micrograph of finely ground talc (<20 μm). It can be observed that each particle is constituted by several individual sheets stacked one on top of the other. The mean thickness of talc particles is 0.266 ± 0.173 μm. This value was obtained by measuring approximately 500 particles.

Figure 4. TEM micrograph of finely ground talc (<20 µm) embedded in a resin and cut perpendicularly to the basal plane of particles.

The results of chemical analyses are presented in Table 1. The macrocrystalline talc under study has a lower SiO_2 content than the most talcs (higher than 50 wt%). This value proceeds from the presence of associated minerals and it is related to the place where talc has been extracted [29]. Moreover, this sample has a MgO content lower than a rock entirely composed of talc (31.80 wt%). According to these results, this talc presents a Si/Mg ratio of 2.74, while the theoretical value obtained from the stoichiometric formula is 1.97. Thus, there are two possible ways for the origin: talc-forming fluids extracted Mg^{2+} from the rock or they supplied Si^{4+} to it. From the microscopic analysis some SiO_2 relics are present (Figure 1a), so that the origin of this talc was probably a rock rich in Mg^{2+} as dunite, previously reported by Fernandez Lima [30], and the fluids captured Si^{4+} from SiO_2 relics.

Table 1. Chemical analysis of finely ground talc (<20 µm).

Components	Percentage (wt %)
SiO_2	41.70
MgO	15.20
Fe_2O_3	1.20
CaO	12.50
MnO	4.05
Al_2O_3	8.00
LOI (1000 °C, 60 min)	17.35

The value for aluminum oxide (Al_2O_3) relates to the chlorite content in the sample, meanwhile the percentage of CaO reveals the presence of calcite. The low SiO_2 content and high amount of CaO and Al_2O_3 confirm the previous results obtained by OM and XRD. The presence of manganese oxide (MnO) in talc is possible since this element can substitute magnesium in octahedral sites within the talc structure. Chidester et al. [31] reported a similar MnO percentage to that determined for argentinean talc in samples from the United States. Iron content is an effective parameter in the use of talc since it affects its color and brightness [32]. Its percentage, origin (i.e., from crystal structure or from other iron-bearing minerals), and valence forms are important. For this talc sample the Fe_2O_3 content is 1.2 wt%. This value is not unusual in talc, which can be associated with substitutions of Fe in the octahedral site for Mg (as chlorite) or the presence as oxides itself [33].

Loss on ignition (LOI) for this talc sample, which indicates the weight percent of the sample that was volatilized in the furnace, is also included in Table 1. This value is high since it is related to the presence of carbonates and other clay minerals such chlorite, as it was reported by Pi-Puig, Animas-Torices and Solé [34].

From the obtained results by XRF and XRD it can be inferred that the studied talc sample is composed approximately of 80 wt% talc. Several authors demonstrate that talc purity can be upgraded by removing associated minerals and iron oxides through acid leaching [35–38].

Figure 5 shows the FTIR spectra of talc which includes the band assignment to the corresponding minerals. In the -OH stretching region (3400–3800 cm^{-1}), three bands can be detected. The signal at 3677 cm^{-1} corresponds to the interactions of Mg$_3$-OH where all the -OH groups present identical surroundings, bound to three octahedral cations (Mg^{2+}) as their nearest neighbors. The high frequency of this vibration is characteristic of a strong -OH bond with little or no hydrogen bonding. Bands at 3660 and 3643 cm^{-1} are related to the partial replacement of Mg^{2+} by Fe^{2+}/Fe^{3+} and they correspond to possible combinations of the two different cations within the octahedral sites [39]. Considering that the wavenumber of -OH stretching is affected by the nature of the cations (electronegativity, atomic mass, size, etc.) and by the total charge in the octahedral sheet, the replacement by Fe^{2+}/Fe^{3+} lowers the band vibrational frequency with respect to the corresponding Mg$_3$-OH. In this sense, the band at 3660 cm^{-1} is associated with Mg$_2$Fe-OH and at 3643 cm^{-1} is related to MgFe$_2$-OH. In the region 400–1300 cm^{-1}, the spectrum shows well-defined absorption talc bands. At 1017 cm^{-1} the stretching vibration of Si-O-Si bonds is detected, meanwhile the deformation of -OH is observed at 670 cm^{-1}. In addition, there are bands at 533 and 451 cm^{-1} which are associated with Si-O-Mg vibration, at 465 cm^{-1} to Mg-O and at 425 cm^{-1} to Si-O. Besides talc bands, this sample contains associated minerals such as chlorite (3687 and 3431 cm^{-1}), calcite and dolomite (2926, 2532, 1440 and 884 cm^{-1}), and magnesite (1440, 884 and 747 cm^{-1}).
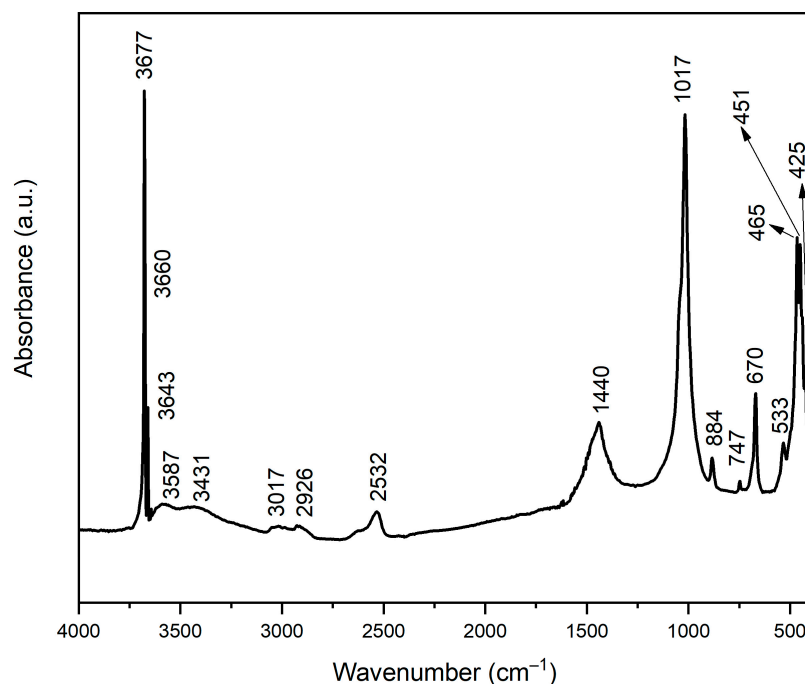

Figure 5. FTIR spectra of finely ground talc (<20 μm).

TG and DTG curves of talc are shown in Figure 6 where mass loss and degradation temperature are included for each event. It can be observed that the sample suffers three mass losses up to 1000 °C. This sample does not contain physically adsorbed water since its mass is constant up to 150 °C. The first and most important mass loss (10.17%) begins at 400 °C and corresponds to the thermal decomposition of chlorite (dehydroxylation reaction) [40]. At 600 °C, magnesite starts to decompose thermally. From 800 °C several thermal decompositions occur and the corresponding mass loss is overlapped. In this sense, talc begins to decompose into enstatite (MgSiO$_3$) and silica minerals (SiO$_2$) [41], but

also dolomite and calcite start to be decomposed [42]. The total mass loss corresponds to 15.58%, which is very similar to the LOI value obtained by the chemical analysis (Table 1), as expected.
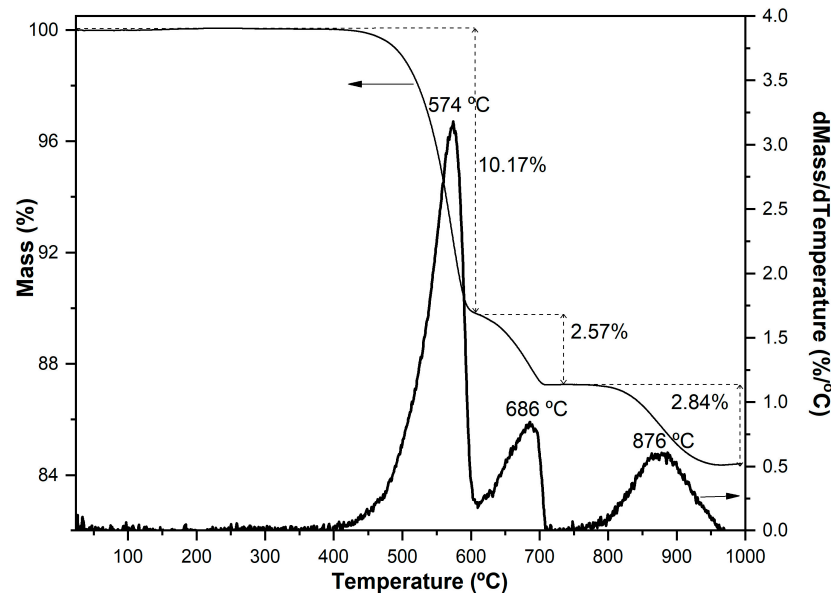

Figure 6. TG and DTG curves of finely ground talc (<20 μm).

Color is one of the most important properties for evaluating talc commercial value. It is associated with the extent of light reflection–diffusion on the mineral surface, which depends on grain size, grain shape, and particle roughness, as well as chemical composition [28,32,43–46]. Color parameters for the studied talc in the CIELAB (Commission Internationale de l´Eclairage *L*a*b**) system are *L** = 82.76, *a** = −1.50, and *b** = 5.38; where *L** ranges from 100 (white) to 0 (black), *a** from −*a** (green) to +*a** (red), and *b** from −*b** (blue) to +*b** (yellow). These results reveal a green chromatic component and a slight yellowing, confirming the observations made with the naked eye. The color of the studied talc could be attributed to the presence of associated minerals such as chlorite or traces of Fe oxides [40,47,48]. It has been reported that chlorite contains chromophore elements in its structure [49–52] and it is responsible for the greenish and yellowish colors in commercial talc. The presence of magnesium carbonates such as magnesite and dolomite could induce a darkening by lowering the *L** value. Concerning the calcium carbonate influence on color parameters, it was reported that it has a less total effect than the other carbonates [48]. The whiteness index (*WI*) value for this talc is 62.12, which impedes its commercialization as a high-priced mineral (*WI* higher than 91%) for paper, cosmetics, and ceramic applications.

Although some features of this talc sample restrict its use in the aforementioned applications, it can be employed as a very efficient filler for plastics. Talc particles can be suitable for most traditional processes of plastic products such as extrusion blow molding, injection molding, extrusion molding and compression molding, among others, without having to upgrade or change the equipment or the production technology. At the beginning, talc particles were mixed with polymers to reduce costs, but later it was demonstrated that there were other advantages related to material performance. In this sense, talc particles influence mechanical, thermal, optical, and barrier properties of polymers [53,54]. Regardless of its crystalline morphology, talc acts as a nucleating agent since its basal surfaces offer active sites to nucleate polymer crystals [55]. This allows improving the productivity as talc particles accelerate the cooling rate of plastic compounds. Particularly, macrocrystalline talc has a higher surface than the microcrystalline one where thicker crystals can be epitaxially grown. The induction of these specific crystals with distinctive mechanical properties is different from those induced by other mineral particles, even for microcrystalline talc [56]. In addition, it promotes a high polymer chain orientation as a

consequence of particle preferential spatial distribution during processing. Macrocrystalline talc improves light barrier properties since particle orientation in polymer matrices blocks the light transmission. The enhancement of gas barrier properties is given by the tortuous path that particles offer to gas diffusion, but also by the crystals that they induce and the hydrophobic character of its basal surfaces. Concerning the color parameters of this talc sample, this is not a critical aspect for plastic products since different pigments can be incorporated during the manufacturing. Moreover, it was demonstrated that associated minerals such as iron impurities could act as promoters of polymer degradation. In this way, this talc sample is a good environmentally friendly alternative as a pro-degradant additive for polymer degradation due to its low cost and sustainability, since it does not contain heavy metals [57]. On the other hand, an integrated purification process was proposed in order to remove mainly the iron oxides [58]. When this process is applied in a macrocrystalline talc, a purified mineral is obtained, conserving its morphological characteristics (i.e., macrocrystalline character).

4. Conclusions

An integral characterization was performed on an argentinean talc ore, analyzing petrographical, mineralogical, morphological, geochemical and physicochemical features by complementary and independent techniques. The deposit, located in the San Juan province at the foothills of the Andes, contains talc interlaminated with chlorite and carbonates (magnesite, calcite, and dolomite) in the form of veins. Moreover, some iron oxides and quartz relics were distinguished in talc ore. From this last finding it could be inferred that the talc origin was probably a rock rich in Mg^{2+} and the talc-forming fluids captured Si^{4+} from SiO_2 relics. Both the talc macrocrystalline character and high crystallinity probably resulted from the surrounding pressure during its formation in the Upper Paleozoic–Lower Triassic. Color properties of this talc, derived from the chlorite and iron oxides presence, restricts its commercialization as a high-priced mineral and to be used for paper, cosmetics, and ceramic applications. However, it can be employed as a filler for plastics since talc acts as a nucleating agent since its basal surfaces offer active sites to nucleate polymer crystals. Particularly, macrocrystalline talc has a higher efficiency as a nucleator than a microcrystalline one, leading to a notable improvement in the mechanical, thermal, optical, and barrier properties of polymers. Moreover, the presence of iron impurities in this talc could promote the polymer degradation, being an environmentally friendly alternative to the commonly used degradants that contain heavy metals. On the other hand, these impurities could be removed by a sustainable purification method without changing the macrocrystalline character. For the aforementioned characteristics and properties, macrocrystalline Argentinean talc has the potential to be used as filler in semicrystalline polymers since the final properties are better than those induced by microcrystalline ones.

Author Contributions: L.A.C. performed the experimental work and wrote the paper; S.E.B. assisted with the writing and the interpretation and discussion of the obtained results. All authors have read and agreed to the published version of the manuscript.

Data Availability Statement: The data presented in this study are available within the article.

Conflicts of Interest: The authors declare no conflict of interest.

References

1. Bowen, N.L.; Tuttle, O.F. The system MgO-SiO_2-H_2O. *Bull. Geol. Soc. Am.* **1949**, *60*, 439–460. [CrossRef]
2. Yoder, H.S. The MgO-$Al2O_3$-SiO_2-H_2O system and related metamorphic facies. *Am. J. Sci.* **1952**, 569–627.

3. Malhammar, G. Determination of some surface properties of talc. *Colloids Surf.* **1990**, *44*, 61–69. [CrossRef]
4. Fuerstenau, M.C.; López Valdiviezo, A.; Fuerstenau, D.W. Role of hydrolyzed cations in the natural hydrophobicity of talc. *Int. J. Miner. Proc.* **1988**, *23*, 161–170. [CrossRef]
5. Chander, S.; Wie, J.M.; Fuerstenay, D.W. On the native floatability and surface properties of naturally hydrophobic solids. In *Advances in Interfacial Phenomena*; Somasundaran, P., Ed.; AIChE: New York, NY, USA, 1975; Series N° 150; pp. 183–188.
6. Pugh, R.J.; Tjus, K. Flotation depressant action of poly(oxyethylene) alkyl ethers on talc. *Colloids Surf.* **1990**, *47*, 179–184. [CrossRef]
7. Yariv, S. Wettability of Clay Minerals. In *Modern Approaches to Wettability: Theory and Applications*; Schrader, M.E., Loeb, G., Eds.; Plenum Press: New York, NY, USA, 1992; pp. 279–326.
8. Ciullo, P.A. *Industrial Minerals and Their Uses: A Handbook and Formulary*; Noyes Publications: Saddle River, NJ, USA, 1996; pp. 68–72.
9. Rayner, J.H.; Brown, G. The crystal structure of talc. *Clay Clay Miner.* **1973**, *13*, 73–84. [CrossRef]
10. Bragg, L.; Claringbull, G.F. *Crystal Structures of Minerals*; G. Bell and Sons, Ltd.: London, UK, 1965.
11. What Is Talc? Geology and Occurrence. Available online: https://www.eurotalc.eu/what-is-talc/geology-and-occurrence/ (accessed on 21 February 2023).
12. Sibelco. Available online: https://coatings.sibelcotools.com/mineral/talc/ (accessed on 21 February 2023).
13. Caminos, R. Geología de la vertiente oriental del Cordón del Plata, Cordillera Frontal de Mendoza. *Revista de la Asociación Geol. Argent.* **1965**, *20*, 351–392.
14. Gregori, D.A. Permo-Triassic volcanic-arc granites in the Mendoza Frontal Cordillera, Argentina. In Proceedings of the XVII Simposio Sobre la Geología de Latinoamérica, Stuttgart, Germany, 13 October 2000.
15. Gregori, D.A.; Fernandez-Turiel, J.L.; Lopez-Soler, A.; Petford, N. Geochemistry of Upper-Palaeozoic-Lower Triassic granitoids of Central Frontal Cordillera, Argentina. *J. S. Am. Earth Sci.* **1996**, *9*, 141–151. [CrossRef]
16. Rapela, C.W.; Pankhurst, R.J.; Casquet, C.; Baldo, E.G.; Galindo, C.; Fanning, C.M.; Dahlquist, J.M. The Western Sierras Pampeanas: Protracted Grenville-age history (1330–1030 Ma) of intra-oceanic arcs, subduction–accretion at continental-edge and AMCG intraplate magmatism. *J. S. Am. Earth Sci.* **2010**, *29*, 105–127. [CrossRef]
17. SEGEMAR-UNSAM. *Talco y Pirofilita*; Technical note; Servicio Geológico Minero Argentino: Buenos Aires, Argentina, 2005.
18. Hunter, R.S. New Reflectometer and Its Use for Whiteness Measurement. *J. Opt. Soc. Am.* **1960**, *50*, 44–48. [CrossRef]
19. Stensby, P.S. Optical Brighteners and Their Evaluation. *Soap Chem. Spec.* **1967**, *97*, 41–44.
20. Bailey, S.W. X-ray diffraction identification of the polytypes of mica, serpentine, and chlorite. *Clay Clay Miner.* **1988**, *36*, 193–213. [CrossRef]
21. Bons, A.J.; Schryvers, D. High-resolution electron microscopy of stacking irregularities in chlorites from the central Pyrenees. *Am. Miner.* **1989**, *74*, 1113–1123.
22. Warr, L.N. Recommended abbreviations for the names of clay minerals and associated phases. *Clay Miner.* **2020**, *55*, 261–264. [CrossRef]
23. Holland, H.J.; Murtagh, M.J. An XRD morphology index for talcs: The effect of particle size and morphology on the specific surface area. *Int. Cent. Diffr. Data Adv. X-ray Anal.* **2000**, *42*, 421–428.
24. Arai, Y. *Chemistry of Powder Production*; Chapman & Hall: London, UK, 1996.
25. Chinnery, N.J.; Pawley, A.R.; Clark, S.M. In situ observation of the formation of 10 Å phase from talc+ H_2O at mantle pressures and temperatures. *Science* **1999**, *286*, 940–942. [CrossRef]
26. Balek, V.; Šubrt, J.; Pérez-Maqueda, L.A.; Beneš, M.; Bountseva, I.M.; Beckman, I.N.; Pérez-Rodríguez, J.L. Thermal behavior of ground talc mineral. *J. Min. Metall.* **2008**, *44*, 7–17. [CrossRef]
27. Steen, W. *Handbook of Polypropylene and Polypropylene Composites*; Karian, H., Ed.; Wiley: Hoboken, NJ, USA, 1999.
28. Ciullo, P.A.; Robinson, S. Talc Shape and Form Meet Function. *Paint Coat. Ind.* **2003**, *1*, 30–33.
29. Lugwisha, E.H.J. Properties of fired bodies made from Tanzanian talc-clay mixes for ceramic applications. *Tanzan. J. Sci.* **2006**, *32*, 69–79. [CrossRef]
30. Fernández Lima, J.C. *Informe Sobre la Mina de Talco de la Quebrada Agua del Gato*; Departamento Angaco-Provincia de San Juan, Ministerio de Economía de la Nación, Secretaría de Industria y Minería, Subsecretaría de Minería, Dirección Nacional de Geología y Minería: Buenos Aires, Argentina, 1962.
31. Chidester, A.H.; Engel, A.E.J.; Wright, L.A. *Talc Resources of the United States (Geological Survey Bulletin 1167)*; US Government Printing Office: Washington, DC, USA, 1964; pp. 1–61.
32. Bundy, W.M.; Ishley, J.N. Kaolin in paper filling and coating. *Appl. Clay Sci.* **1991**, *5*, 397–420. [CrossRef]
33. Buzon, M.E.; Gunter, M.E. Current issues with the purported "asbestos" content of talc: Hydrothermal-hosted talc ores in southwest Montana. *Trans. Soc. Min. Metall. Explor.* **2017**, *342*, 62–71. [CrossRef]
34. Pi-Puig, T.; Animas-Torices, D.Y.; Solé, J. Mineralogical and geochemical characterization of talc from two mexican ore deposits (oaxaca and puebla) and nine talcs marketed in mexico: Evaluation of its cosmetic uses. *Minerals* **2020**, *10*, 388. [CrossRef]
35. Castillo, L.A.; Barbosa, S.E.; Maiza, P.; Capiati, N.J. Surface modifications of talcs. Effects of inorganic and organic acid treatments. *J. Mater. Sci.* **2011**, *46*, 2578–2586. [CrossRef]
36. Ahmed, M.M.; Ibrahim, G.A.; Hassan, M.M. Improvement of Egyptian talc quality for industrial uses by flotation process and leaching. *Int. J. Miner. Process.* **2007**, *83*, 132–145. [CrossRef]

37. Orosco, R.P.; Ruiz, M.D.C.; Barbosa, L.I.; González, J.A. Purification of talcs by chlorination and leaching. *Int. J. Miner. Process.* **2011**, *101*, 116–120. [CrossRef]

38. Barani, K.; Aghazadeh, V. Removal of impurities from talc ore by leaching method. *J. Chem. Technol. Metall.* **2018**, *53*, 296–300.

39. Farmer, V.C. The layer silicates. In *The Infrared Spectra of Minerals*; Farmer, V.C., Ed.; Mineralogical Society: London, UK, 1974; pp. 331–363.

40. Ersoy, B.; Dikmen, S.; Yildiz, A.; Gören, R.; Elitok, Ö. Mineralogical and physicochemical properties of talc from Emirdağ, Afyonkarahisar, Turkey. *Turk. J. Earth Sci.* **2013**, *22*, 632–644. [CrossRef]

41. Nkoumbou, C.; Njopwouo, D.; Villiéras, F.; Njoya, A.; Ngouné, C.Y.; Ndjock, L.N.; Tchoua, F.M.; Yvon, J. Talc indices from Boumnyebel (Central Cameroon), physico-chemical characteristics and geochemistry. *J. Afr. Earth Sci.* **2006**, *45*, 61–73. [CrossRef]

42. Földvári, M. *Handbook of Thermogravimetric System of Minerals and Its Use in Geological Practice*; Geological Institute of Hungary: Budapest, Hungary, 2011; Volume 213, pp. 1–180.

43. Billmeyer, F.W.; Saltzman, M. *Principles of Color Technology*, 2nd ed.; Wiley-Interscience: New York, NY, USA, 1981.

44. Zazenski, R.; Ashton, W.H.; Briggs, D.; Chudkowski, M.; Kelse, J.W.; Maceachern, L.; Mccaarthy, E.F.; Nordhauser, M.A.; Roddy, M.T.; Teetsel, N.M.; et al. Talc: Occurrence, characterization, and consumer applications. *Regul. Toxicol. Pharmacol.* **1995**, *21*, 218–229. [CrossRef]

45. Bizi, M.; Flament, M.P.; Baudet, G.; Gayot, A. Relation between structural characteristics of talc and its properties as an antisticking agent in the production of tablets. *Eur. J. Pharm. Sci.* **2003**, *19*, 373–379. [CrossRef]

46. Gamiz, E.; Melgosa, M.; Sanchez-Maranon, M.; Martin, M.J.M.; Delgado, R. Relationships between chemicomineralogical composition and color properties in selected natural and calcined Spanish kaolins. *Appl. Clay Sci.* **2005**, *28*, 269–282. [CrossRef]

47. Deer, W.A.; Howie, R.A.; Zussman, J. *An Introduction to the Rock-Forming Minerals*; Longman Scientific & Technical: Essex, UK, 1992.

48. Soriano, M.; Sanchez-Maranon, M.; Melgosa, M.; Gamiz, E.; Delgado, R. Influence of chemical and mineralogical composition on colour for commercial talcs. *Color Res. Appl.* **2002**, *27*, 430–440. [CrossRef]

49. Burns, R.G. Mineralogical applications of crystal field theory. In *Cambridge Topics in Mineral Physics and Chemistry*, 2nd ed.; Cambridge University Press: Cambridge, UK, 1993.

50. Smith, G. Low-temperature optical studies of metal-metal charge transfer transitions in various minerals. *Can. Miner.* **1977**, *15*, 500–507.

51. Bailey, S.W. Chlorites: Structures and crystal chemistry. In Hydrous phyllosilicates (exclusive of micas). *Rev. Miner.* **1988**, *19*, 347–403.

52. Bakhtin, A.I. The distribution of Fe ions in chlorites. *Geochem. Int.* **1986**, *23*, 63–67.

53. Buzarovska, A.; Bogoeva-Gaceva, G.; Fajgar, R. Effect of the talc filler on structural, water vapor barrier and mechanical properties of poly (lactic acid) composites. *J. Polym. Eng.* **2016**, *36*, 181–188. [CrossRef]

54. Mittal, V. Mechanical and Gas Barrier Properties of Polypropylene Layered Silicate Nanocomposites: A Review. *Open. Macromol. J.* **2012**, *6*, 37–52. [CrossRef]

55. Castillo, L.A.; Barbosa, S.E. Comparative analysis of crystallization behavior induced by different mineral fillers in polypropylene nanocomposites. *Nanomater. Nanotechnol.* **2020**, *10*, 1847980420922752. [CrossRef]

56. Castillo, L.A.; Barbosa, S.E.; Capiati, N.J. Influence of talc morphology on the mechanical properties of talc filled polypropylene. *J. Polym. Res.* **2013**, *20*, 152. [CrossRef]

57. Linares, P.B.; Castillo, L.A.; Barbosa, S.E. Pro-degradant effect of talc nanoparticles on polypropylene films. *J. Polym. Environ.* **2019**, *27*, 1666–1676. [CrossRef]

58. Castillo, L.A.; Barbosa, S.E.; Maiza, P.; Capiati, N.J. Integrated process for purification of low grade talc ores. *Part. Sci. Technol.* **2014**, *32*, 1–7. [CrossRef]